PHOTOSYSTEM II PROTEIN33, a Protein Conserved in the Plastid Lineage, Is Associated with the Chloroplast Thylakoid Membrane and Provides Stability to Photosystem II Supercomplexes in Arabidopsis[1][OPEN]

Rikard Fristedt, Andrei Herdean, Crysten E. Blaby-Haas, Fikret Mamedov, Sabeeha S. Merchant, Robert L. Last, and Björn Lundin*

Department of Chemistry and Biochemistry (R.F., C.E.B.-H., S.S.M.) and Institute for Genomics and Proteomics (S.S.M.), University of California, Los Angeles, California 90095; Department of Biological and Environmental Sciences, University of Gothenburg, 405 30 Gothenburg, Sweden (A.H., B.L.); Department of Chemistry, Ångström Laboratory, Uppsala University, 751 20 Uppsala, Sweden (F.M.); and Department of Biochemistry and Molecular Biology and Department of Plant Biology, Michigan State University, East Lansing, Michigan 48824 (R.L.L., B.L.)

ORCID IDs: 0000-0002-2594-509X (S.S.M.); 0000-0001-6974-9587 (R.L.L.).

Photosystem II (PSII) is a multiprotein complex that catalyzes the light-driven water-splitting reactions of oxygenic photosynthesis. Light absorption by PSII leads to the production of excited states and reactive oxygen species that can cause damage to this complex. Here, we describe Arabidopsis (*Arabidopsis thaliana*) At1g71500, which encodes a previously uncharacterized protein that is a PSII auxiliary core protein and hence is named *PHOTOSYSTEM II PROTEIN33* (*PSB33*). We present evidence that PSB33 functions in the maintenance of PSII-light-harvesting complex II (LHCII) supercomplex organization. *PSB33* encodes a protein with a chloroplast transit peptide and one transmembrane segment. In silico analysis of PSB33 revealed a light-harvesting complex-binding motif within the transmembrane segment and a large surface-exposed head domain. Biochemical analysis of PSII complexes further indicates that PSB33 is an integral membrane protein located in the vicinity of LHCII and the PSII CP43 reaction center protein. Phenotypic characterization of mutants lacking PSB33 revealed reduced amounts of PSII-LHCII supercomplexes, very low state transition, and a lower capacity for nonphotochemical quenching, leading to increased photosensitivity in the mutant plants under light stress. Taken together, these results suggest a role for PSB33 in regulating and optimizing photosynthesis in response to changing light levels.

PSII is a multiprotein complex in plants with 31 identified polypeptides (Wegener et al., 2011; Pagliano et al., 2013). It is associated with an extrinsic trimeric light-harvesting complex (LHC), forming the PSII-LHCII supercomplex. The PSII complex performs a remarkable biochemical reaction, the oxidation of water using light energy from the sun, which profoundly contributes to the overall biomass accumulation in the biosphere (Barber et al., 2004). Consequently, the stability and functional integrity of the PSII-LHCII supercomplex is crucially important for photosynthetic function. The energy of a photon, either absorbed directly by PSII or indirectly via energy transfer from adjacent antenna chlorophyll (Chl) molecules, excites the PSII reaction center P680. The excited state, P680*, can transfer an electron to pheophytin, producing the most powerful oxidant known in biology, $P680^+$, which can remove electrons from water. Excessive input of excitation energy into PSII saturates the electron transfer system and causes either acceptor or donor site limitation in the complex. This results in increased production of reactive oxygen species (ROS): singlet oxygen at the PSII donor side and superoxide at the acceptor side (Munné-Bosch et al., 2013). Several protective mechanisms have been documented that decrease the production of singlet oxygen at the PSII donor side in photosynthetic eukaryotes. Notably, reducing energy transfer from LHC to PSII

[1] This work was supported by the National Science Foundation Arabidopsis 2010 Project (grant nos. MCB–0519740 and MCB–1119778 to R.L.L.); by the Wilhelm and Martina Lundgrens Foundation, Gothenburg University, the Wallenberg Foundation, the Lars Hiertas Foundation, and the Helge Axel Ax:son Foundation (all to B.L.); by the Wenner-Gren Foundation (to R.F.); by the Wallenbergs Foundation and the Swedish Energy Authority (to F.M.); by the Office of Science (Biological and Environmental Research), U.S. Department of Energy (grant no. DE–FC02–02ER63421); by the Kirschstein National Research Service Award from the National Institutes of Health (grant no. GM100753 to C.E.B.-H.); and by the Lady Davis Foundation of the Hebrew University in Jerusalem, Israel, and the Weizmann Institute of Science in Rehovot, Israel (sabbatical support to R.L.L.).

* Address correspondence to bjorn.lundin@gmail.com.

The author responsible for distribution of materials integral to the findings presented in this article in accordance with the policy described in the Instructions for Authors (www.plantphysiol.org) is: Björn Lundin (bjorn.lundin@gmail.com).

[OPEN] Articles can be viewed without a subscription.
www.plantphysiol.org/cgi/doi/10.1104/pp.114.253336

via nonphotochemical quenching (NPQ) is a key avoidance mechanism (Ruban and Murchie, 2012).

Despite years of intensive study of PSII structure and function, new proteins that are associated with the PSII complex continue to be discovered, including an increasing number involved in the stability and organization of PSII-LHCII supercomplexes (García-Cerdán et al., 2011; Lu et al., 2011a; Wegener et al., 2011). Two complementary approaches (Merchant et al., 2007; Lu et al., 2008, 2011b; Ajjawi et al., 2010) that utilize phylogenomics (GreenCut) and large-scale phenotypic mutant screening (Chloroplast 2010 Project; http://www.plastid.msu.edu/) were employed by our groups to discover novel plant proteins with roles in photosynthesis. GreenCut identifies proteins found only in photosynthetic organisms, and it is likely that many of them are involved in biochemical processes associated with the structure, assembly, or function of the photosynthetic apparatus and the chloroplast that houses it (Merchant et al., 2007; Karpowicz et al., 2011). The Chloroplast 2010 Project was a large-scale reverse-genetic mutant screen in which thousands of homozygous Arabidopsis (*Arabidopsis thaliana*) transfer DNA (T-DNA) insertion lines were analyzed for defects in the rise and decay kinetics of Chl fluorescence (Lu et al., 2008, 2011a, 2011b; Ajjawi et al., 2010).

The GreenCut and Chloroplast 2010 approaches both identified the Arabidopsis At1g71500 locus as encoding a protein of unknown function with potential relevance to photosynthesis. In this work, we demonstrate that plant lines carrying three independent mutations at this locus display severe light-induced photoinhibition due to a less stable supramolecular organization of PSII. Biochemical analyses revealed that this protein is associated with PSII complexes, and since the last described PSII protein was called PHOTOSYSTEM II PROTEIN32 (PSB32), we named the gene *PSB33*. The nuclear genome-encoded PSB33 is predicted to have a chloroplast transit peptide and a transmembrane domain. The biochemical analyses presented below indicate that PSB33 is required for the proper interaction and stability of PSII-LHCII supercomplexes and, in turn, in regulating photosynthesis in response to fluctuating light levels.

RESULTS

Identification of the *PSB33* Gene

A mutant of At1g71500 was identified as part of the Chloroplast 2010 functional genomics pipeline (Lu et al., 2008, 2011a, 2011b; Ajjawi et al., 2010). Over 5,200 Arabidopsis homozygous T-DNA lines were screened for altered Chl fluorescence in plants grown under a photosynthetic photon flux density (PPFD) of either 100 or 1,000 μmol photons m^{-2} s^{-1}. The Chloroplast 2010 Project identified the SALK_098173 mutant (now called *psb33-1*) as having a very low maximal PSII quantum yield (F_v/F_m) following 3 h of photoinhibiting light (1,000 PPFD). Examination of the expression of *PSB33* from transcriptome sequencing studies in Arabidopsis (Bernal et al., 2012) revealed that *PSB33* had a similar transcript abundance to other auxiliary PSII subunits (Supplemental Table S1). These results led to the hypothesis that the mutant was impacted in PSII function.

Several lines of evidence confirm that the phenotype is due to a mutation of At1g71500. First, photosynthetic defects were found for homozygous mutants with two additional alleles, *psb33-2* (Cold Spring Harbor Laboratory [GABL]_GT25677) and *psb33-3* (German Plant Genomics Research Program [GABI]_574D02; Fig. 1, A and B). Second, introduction of the native *PSB33* gene into *psb33-1* by *Agrobacterium tumefaciens*-mediated transformation (*psb33-1-C*; Fig. 1D; Supplemental Fig. S1A) restored PSB33 abundance and reversed the *psb33* mutant growth and PSII supercomplex accumulation phenotypes (Supplemental Fig. S1, B and C). To test the hypothesis that the subcellular localization of the protein is consistent with a function in the light reactions of photosynthesis, anti-PSB33 antibodies were generated as described in "Materials and Methods." These antibodies recognized a protein from leaf extracts of wild-type plants that migrates under SDS and urea denaturing PAGE consistent with a molecular mass of 23 kD. The protein was not detected in extracts from *psb33-2* and *psb33-3*, demonstrating antibody specificity (Fig. 1C). The complemented line accumulates the protein to levels comparable to wild-type plants (Supplemental Fig. S1A). Also, the partial loss-of-function *psb33-1* allele, which has a T-DNA insertion in the 5′ untranslated region (UTR), showed an 85% reduction compared with the wild-type amount of PSB33 (Fig. 1C). The severity of the slow-growth phenotype of the mutants correlated well with the degree of protein reduction, with the growth of the *psb33-1* mutant intermediate to that of the wild type and the two protein-coding sequence insertion mutants (Fig. 1D).

The total Chl contents and Chl *a/b* ratios of the mutant plants are slightly lower than those of wild-type plants (Table I), suggesting minor changes in the abundance of the Chl-containing complexes in the mutant plants in vivo. However, levels of LHC, PSII, PSI, cytochrome b_6f complex, and ATPase synthase proteins detected by immunodetection, heme-specific staining, and two-dimensional (2D) blue native/SDS-PAGE coupled with mass spectrometry showed no significant differences between *psb33-1* mutant and wild-type plants under nonstressful standard growth light conditions (Fig. 2; Supplemental Fig. S2).

Sequence Analysis of PSB33 and Related Proteins

A search for homologs of Arabidopsis PSB33 among the plant and algal genomes available in the National Center for Biotechnology Information database revealed one or two homologs of PSB33 (Supplemental Fig. S3, A and C). PSB33 and orthologs share similarity with Rieske-type proteins, and the highest scoring structural homolog to PSB33 in the Protein Data Bank is the Rieske-type nonheme iron monooxygenase from *Pseudomonas putida* (Martins et al., 2005). However, neither the iron-sulfur-binding residues nor the mononuclear iron-binding

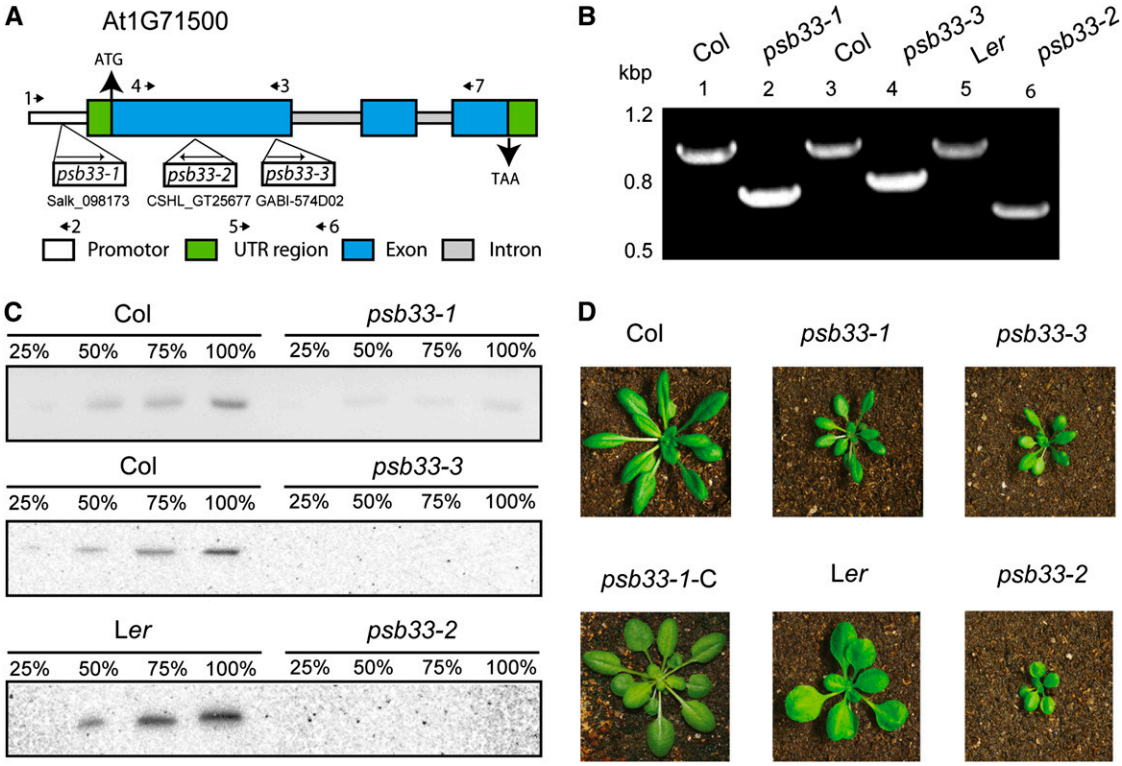

Figure 1. Loss of PSB33 results in an altered growth phenotype. A, Localization of T-DNA insertion sites in *PSB33* DNA. Three *psb33* alleles are shown: *psb33-1*, *psb33-2*, and *psb33-3*. The *PSB33* genomic DNA contains three exons (blue boxes) and two introns (gray boxes). Green boxes represent the 5′ and 3′ UTRs, and the white line represents the 5′ flanking sequence. B, PCR products obtained from genomic DNA with the following set of primers (numbered as in A): 1 to 3 (lanes 1 and 2); 4, 5, and 7 (lanes 3 and 4); and 4, 6, and 7 (lanes 5 and 6), separated on agarose gels and stained with ethidium bromide. C, Immunodetection of PSB33 abundance. PSB33 levels were analyzed in wild-type Columbia-0 (Col), *psb33-1*, *psb33-3*, wild-type Landsberg *erecta* (L*er*), and *psb33-2* plants. Protein extracts from whole leaf were probed with a PSB33-specific antibody. D, Phenotypes of wild-type and mutant plants. Plants were grown for 3 weeks under normal light conditions (120 PPFD) with a day/night cycle of 16 h of light/8 h of dark.

site is present in PSB33 (Supplemental Fig. S3A). PSB33 and orthologs in land plants and algae contain a putative transmembrane region near the C terminus. In land plants, this region includes a partial Chl-binding domain (pfam00504; Punta et al., 2012). The highest scoring BLAST hits of this domain are orthologs of Arabidopsis PSBS (Supplemental Fig. S3B), a protein in the LHC superfamily that is involved in NPQ in land plants.

No orthologs of PSB33 were found in cyanobacteria. Instead, the cyanobacterial genomes analyzed contain a closely related protein that has retained the iron-sulfur-binding residues and lacks the C-terminal extension that is characteristic of PSB33. The algal genomes analyzed encode both an ortholog of PSB33 and an ortholog of this cyanobacterial protein (Supplemental Fig. S3, A and C).

Subcellular Localization and Abundance Show That PSB33 Is Located Close to PSII

To test the hypothesis that PSB33 is a membrane-bound chloroplast protein situated close to PSII, a PSB33-GFP fusion protein was transiently expressed in tobacco (*Nicotiana tabacum*) leaves (GFP at the C terminus). GFP fluorescence and Chl autofluorescence were colocalized (Fig. 3A), indicating that the fusion protein is targeted to the chloroplast. Biochemical fractionation methods were employed to confirm this finding and to further localize the native PSB33 within a subcompartment of the chloroplast. Intact Arabidopsis chloroplasts were isolated by Percoll gradient centrifugation, lysed, and further fractionated by Suc density gradient centrifugation followed by immunodetection using a PSB33-specific antibody. Consistent with the hypothesis that PSB33 is a membrane-associated PSII protein, a signal was detected in membrane-containing and PSII-containing fractions (whole leaf, chloroplast, thylakoid, PSII-enriched membranes, and PSII-LHCII supercomplexes) but not in the soluble chloroplast stroma or thylakoid lumen fractions (Fig. 3B).

The hypothesis that PSB33 is a PSII-associated protein was evaluated by comparing its enrichment in spinach (*Spinacia oleracea*) leaf PSII-LHCII and PSII core complexes relative to that of the PSII core protein CP43 (Barber et al., 2004; Fig. 3C); a similar 1.5-fold enrichment was obtained for the two proteins, suggesting a similar

Table I. *Chl fluorescence parameters and PSII activity*

Chl content, Chl *a/b* ratio (Porra, 2002), and oxygen evolution were obtained from fresh leaves. Minimal fluorescence yield (F_0), F_v/F_m, functional reaction centers per cross-sectional leaf area (RC/ABS), and photosynthetic performance index (PI) were calculated from fast fluorescence induction. Electron transfer rate of PSII (ETRII), quantum yield of PSII (YII), and NPQ were obtained at steady-state light induction. Quenching related to state transitions was calculated from fluorescence measurements. Proton-motive force (PMF), ΔpH, and $\Delta\Psi$ were obtained by measuring the electrochromic band shift. $n = 3$ to 18. Asterisk denotes a significant difference at $P < 0.05$, and ns indicates no significant difference from the wild type at $P \leq 0.05$. –, No data collected or data absence.

Measured Parameters	Col	*psb33-1*	*psb33-3*
Chl (mg g^{-1} fresh wt)	1.95 ± 0.19	1.84 ± 0.23 ns	1.81 ± 0.16 ns
Chl *a/b* (Porra)	3.4 ± 0.01	3.2 ± 0.29 ns	2.3 ± 0.20*
Chl *a/b* (HPLC)	3.4 ± 0.01	–	3.2 ± 0.04*
F_0	3,952 ± 59	5,375 ± 177*	6,045 ± 222*
F_v/F_m	0.83 ± 0.01	0.78 ± 0.01*	0.75 ± 0.02*
ETRII (300, 700, 1,300 PPFD)	38.3 ± 4.3	40.3 ± 2.0 ns	38.3 ± 2.7 ns
	41.5 ± 3.3	51.1 ± 4.1*	49.2 ± 3.6*
	37.6 ± 4.6	49.9 ± 3.2*	41.4 ± 5.9*
YII (300, 700, 1,300 PPFD)	0.53 ± 0.06	0.56 ± 0.03 ns	0.53 ± 0.03 ns
	0.29 ± 0.02	0.39 ± 0.04*	0.35 ± 0.03*
	0.14 ± 0.02	0.18 ± 0.01*	0.15 ± 0.02 ns
NPQ (300, 700, 1,300 PPFD)	0.51 ± 0.10	0.34 ± 0.10*	0.35 ± 0.03*
	1.15 ± 0.05	0.56 ± 0.07*	0.57 ± 0.09*
	1.78 ± 0.11	1.41 ± 0.15*	1.49 ± 0.30*
Quenching related to state transitions (100 PPFD)	0.06 ± 0.01	−0.01 ± 0.01*	−0.02 ± 0.00*
Photochemical quenching (300, 700, 1,300 PPFD)	0.73 ± 0.08	0.79 ± 0.03 ns	0.78 ± 0.03 ns
	0.45 ± 0.03	0.58 ± 0.05*	0.54 ± 0.03*
	0.23 ± 0.03	0.33 ± 0.01*	0.29 ± 0.03*
RC/ABS	0.75 ± 0.02	0.54 ± 0.02*	0.47 ± 0.02*
PMF (170, 670, 1,270, 2,000 PPFD)	5.00 ± 1.40	–	5.77 ± 1.17 ns
	7.87 ± 0.83	–	7.24 ± 0.31 ns
	7.75 ± 0.90	–	7.14 ± 0.33 ns
	7.64 ± 0.86	–	7.01 ± 0.33 ns
ΔpH (170, 670, 1,270, 2,000 PPFD)	3.63 ± 0.97	–	3.37 ± 0.65 ns
	5.64 ± 1.00	–	5.14 ± 0.63 ns
	7.04 ± 1.18	–	6.51 ± 0.69 ns
	7.64 ± 0.86	–	7.01 ± 0.34 ns
$\Delta\Psi$ (170, 670, 1,270, 2,000 PPFD)	1.37 ± 0.49	–	2.39 ± 0.80 ns
	2.23 ± 0.48	–	2.10 ± 0.50 ns
	0.71 ± 0.45	–	0.63 ± 0.63 ns
	–	–	–
PI	1.43 ± 0.09	0.85 ± 0.09*	0.62 ± 0.09*
Oxygen evolution	0.28 ± 0.05	0.14 ± 0.01*	0.13 ± 0.01*

stoichiometry in the PSII protein complex. To identify the specific PSII subcomplexes containing PSB33, thylakoid membranes were separated by blue native PAGE followed by immunodetection using antibodies directed against PSII protein D1 (D1), PSI P700 Chl *a* apoprotein A1 (PsaA), or PSB33 (Fig. 3D). Strikingly, on blue native gels, the ratio of the D1-containing complexes was different in wild-type versus mutant plants, and again, the difference was more dramatic in the plant with the null allele compared with the *psb33-1* plant that retains 15% of the PBS33 (Fig. 3D; Table II). The defect appeared to be specific to PSII, because both the abundance of tested polypeptides in the other complexes and the level of the PSI supercomplex were unaltered in the mutant as monitored on the basis of PsaA accumulation (Fig. 3D). PSB33 was found in most D1-containing PSII subcomplexes (Fig. 3D). Further evidence that PSB33 is a PSII component was obtained by cross-linking PSB33 against surface-exposed thylakoid membrane proteins and by coimmunoprecipitation using anti-PSB33 antibodies (Supplemental Fig. S4). PSB33 was cross-linked to a high-M_r protein complex that included the PSII proteins LHCII, CP43, D2, and D1 (Supplemental Fig. S4A). Coimmunoprecipitation also showed an interaction with CP43 and Lhcb1.3. These findings are consistent with the hypothesis that PSB33 is present in the peripheral region of PSII close to CP43 and LHCII.

PSB33 Topology

To verify the orientation of PSB33 within the thylakoid membrane, we used a gene fusion, which encodes alkaline phosphatase (PhoA) followed by the alpha peptide of β-galactosidase (LacZα) as a topological reporter in *Escherichia coli* (Hamel et al., 2003). This approach relies on the bioenergetic analogy both between the bacterial periplasm positive (*p*) side and the thylakoid lumen, in

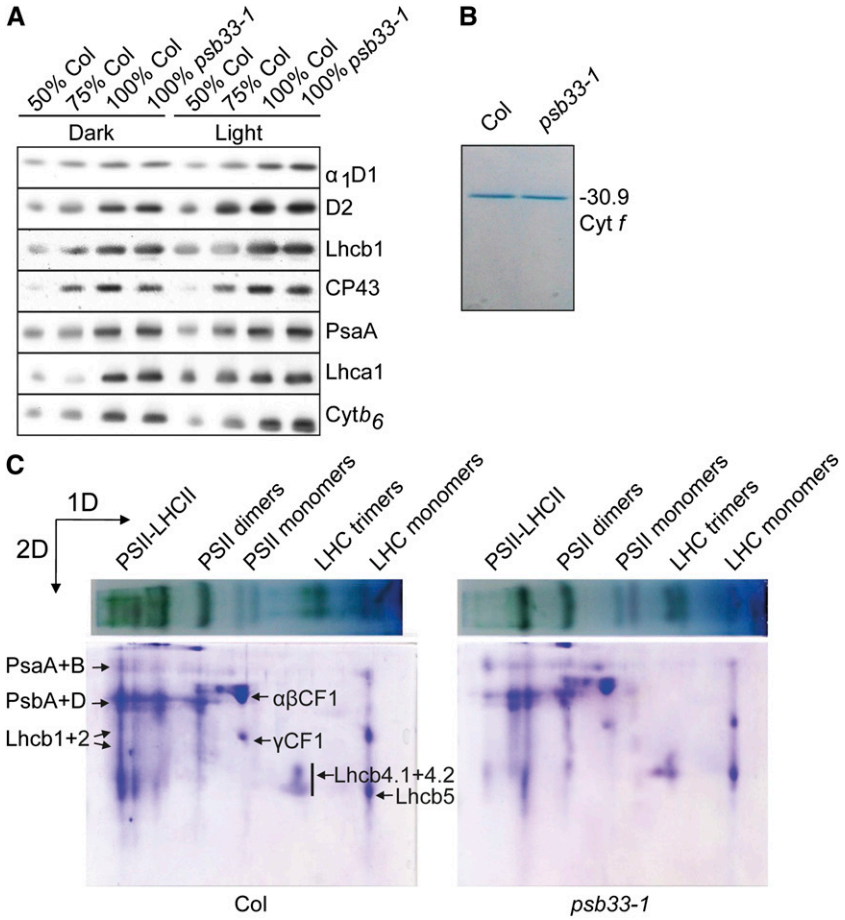

Figure 2. Thylakoid membrane protein abundance. A, Immunodetection of thylakoid membrane proteins. Protein levels were analyzed based on equal loadings of Chl from leaves of 4-week-old wild-type and *psb33* mutant plants. Antibodies used are as indicated at right. B, Identification of the subunits of the heme from the cytochrome *f* complex from total chloroplast proteins. 3,3′,5,5′-Tetramethylbenzidine (TMBZ) heme-specific staining of total chloroplast proteins (Cyt *f*) is shown from wild-type and *psb33-1* mutant plants. C, Absence of PSII supercomplexes in PSB33 mutant plants visualized by blue native PAGE of thylakoid membrane complexes followed by 2D SDS-PAGE. Thylakoid membranes (100 μg of Chl) from 4-week-old wild-type (Col) and *psb33-1* mutant plants exposed to normal light (120 PPFD) for 4 h were solubilized with 0.75% *n*-dodecyl β-D-maltoside and separated on 5% to 13.5% native gradient gels (1D), and the gel lanes were subjected to denaturing SDS-PAGE in the second, vertical dimension (2D). The gels were stained with Coomassie Blue, and the indicated protein spots were identified and verified by in-gel digestion and liquid chromatography-mass spectrometry.

which protons accumulate during active electron transport, and between the bacterial cytoplasm negative (*n*) side and the plastid stroma, which becomes proton deficient. High PhoA activity indicates a *p*-side location of the reporter, while LacZ activity indicates an *n*-side location of the reporter (Hamel et al., 2003; Karamoko et al., 2011). As shown in Supplemental Figure S3D, when the PhoA-LacZα reporter is fused to the N-terminal side of the transmembrane region, transformants display predominantly β-galactosidase activity, suggesting that the Rieske-like domain faces the stroma. Because of the purple coloration of the two C-terminal constructs, we cannot distinguish between a periplasmic localization or insertion of the fusion in a transmembrane region; the latter is supported by I-TASSER (Roy et al., 2010) structure prediction (Supplemental Fig. S3, D and E).

The *psb33* Mutants Display Enhanced Susceptibility to Photoinhibition

We attribute the slow-growth phenotype of *psb33* mutant plants to the impairment of photosynthesis, which is consistent with the physical association of the protein with components of PSII and LHCII and the change in distribution of Chl-containing complexes in the corresponding *psb33* mutant. To further pursue this, we measured photosynthetic electron transfer function under various light conditions. First, the activity of the PSII complex was assessed by measuring oxygen-evolving activity and Chl fluorescence in vivo. Notably, oxygen-evolving activity decreased in the *psb33* mutants even at relatively low light levels (50 PPFD) and was further decreased at higher light intensity (Fig. 4A). This decrease of activity in the mutants could be explained by the observed instability of the PSII-LHCII supercomplexes. Furthermore, consistent with the lower oxygen-evolving activity, the *psb33* mutant plants displayed a lower F_v/F_m ratio compared with wild-type plants (Fig. 4B) both under growth (120) and high (800) PPFD. In line with these results, only a slightly lower F_v/F_m ratio of 0.78 was obtained in dark-acclimated mutant plants compared with 0.83 in the wild-type plants (Table I; Fig. 4B). Additional Chl fluorescence studies monitoring PSII in dark-adapted plants transferred to various light conditions showed that the photochemistry parameter for photochemical quenching was higher in *psb33* mutants than in wild-type plants. This parameter gives an indication that a larger proportion of *psb33* mutant PSII reaction centers stayed open compared with in wild-type plants (Table I). Additionally, *psb33* mutants had an overall higher electron transfer rate (quantum yield of PSII and electron transfer rate of PSII) compared with wild-type plants (Table I). Interestingly, Chl fluorescence studies from

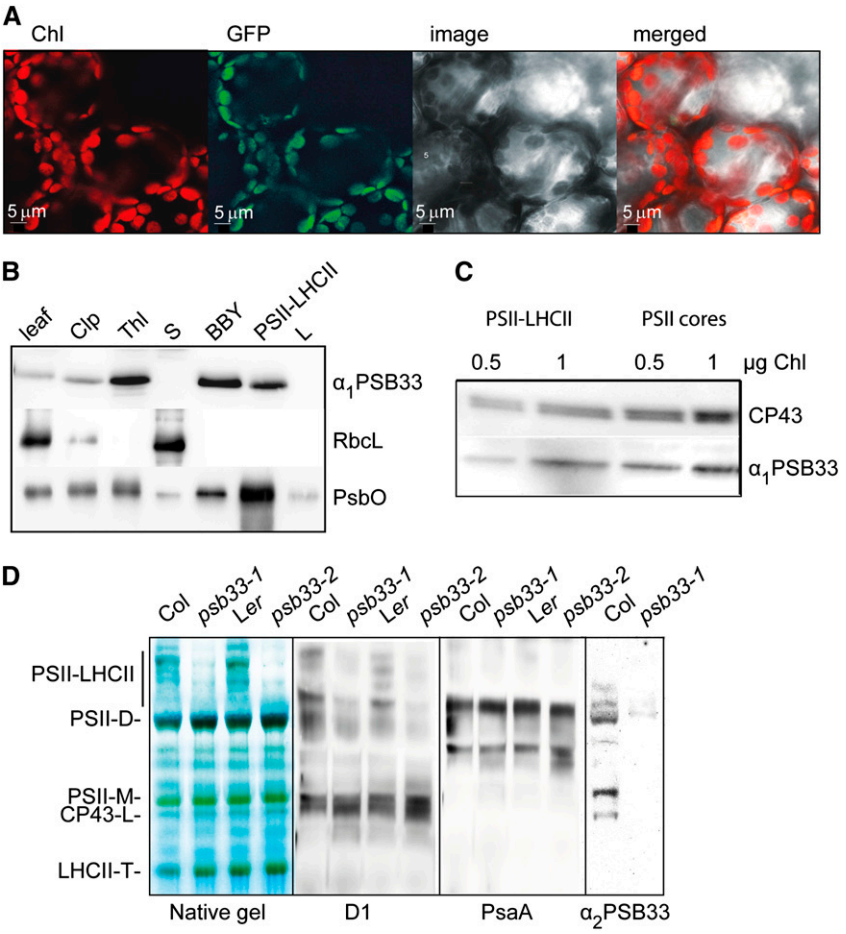

Figure 3. PSB33 is colocalized in thylakoid membranes with PSII-LHCII. A, Chloroplast localization of PSB33. Localization to the chloroplast was demonstrated by confocal images of GFP (green), Chl autofluorescence (red), reflection image (white), and the merged fluorescence image. B, Thylakoid localization of PSB33. Localization of PSB33 was visualized by immunodetection with a PSB33-specific antibody (α_1-PSB33) of extracts from wild-type leaves (leaf), chloroplasts (Clp), thylakoid membranes (Thl), stroma (S), PSII-enriched membranes (BBY), PSII supercomplexes (PSII-LHCII), and the thylakoid lumen (L). The purity of samples was shown by cross reaction with Rubisco (RbscL) and the PSII extrinsic subunit PsbO. C, PSB33 association to PSII. Immunodetection is shown using α_1-PSB33 and CP43 antibody on PSII-LHCII and PSII cores. Chl at 0.5 and 1 μg represent the total amounts of Chl present in samples loaded in each well. D, PSB33 association with native protein complexes. Immunodetection of blue native gels with solubilized thylakoid membranes from wild-type and mutant plants exposed to 120 PPFD for 4 h is shown. Antibodies used from left to right are against D1, PsaA, and PSB33. PSII-LHCII, PSII-LHCII supercomplex; PSI-M, PSI monomer; PSII-D, PSII dimer; PSII-M, PSII monomer; CP43-L, PSII reaction center complex without the CP43 subunit; LHCII-T, LHCII trimer.

light-exposed plants that were subsequently dark adapted showed a lowered electron transfer rate for the PSB33 null mutant compared with wild-type plants (Supplemental Fig. S5D), which correlates well with the slow-growth phenotype. In line with the above results, the abundance of both D1 and CP43 decreased to 80% of the initial value in *psb33-3* (null allele) mutants exposed to 120 PPFD and further decreased to 50% to 60% of dark-acclimated levels following irradiation at 800 PPFD (Fig. 4C). In contrast, wild-type plants maintained dark-acclimated D1 and CP43 levels following a shift from dark to 120 PPFD (growth light). A decrease in wild-type reaction center proteins (to 80% of dark-acclimated levels) was observed only following a shift to 800 PPFD (Fig. 4C).

The above results and the observed whole-plant phenotype show that mutant plants lacking PSB33 are sensitive to light stress conditions. To investigate the relative extent of light-induced oxidative damage to PSII proteins in the *psb33-3* mutant compared with the wild type, we measured ROS accumulation and D1 abundance in light-exposed leaves. Light treatments of 800 PPFD resulted in increased hydrogen peroxide (H_2O_2), superoxide, and singlet oxygen levels in the mutant leaves (Supplemental Fig. S5, A–C) as well as reduced steady-state

Table II. *Protein distribution in various PSII protein complexes*

The total protein contents of D1 and PSB33 in thylakoid membranes are indicated as percentages. The distributions of D1 and PSB33 in PSII protein complexes are estimated by quantitative immunodetection of blue native gels. The results shown are averages of three to five replicates with SD indicated. n.d., Not detected.

Measured Parameters	Col		*psb33-1*		*psb33-2*	
	D1	PSB33	D1	PSB33	D1	PSB33
			%			
Total protein content	100	100	100	15	100	n.d.
PSII-LHCII	38 ± 5	30 ± 6	17 ± 3	28 ± 8	5 ± 5	n.d.
PSII dimers	30 ± 4	20 ± 5	43 ± 6	27 ± 5	62 ± 1	n.d.
PSII monomers	20 ± 2	33 ± 5	25 ± 4	30 ± 2	28 ± 2	n.d.
CP43-less PSII monomers	12 ± 1	17 ± 5	15 ± 4	10 ± 5	5 ± 4	n.d.

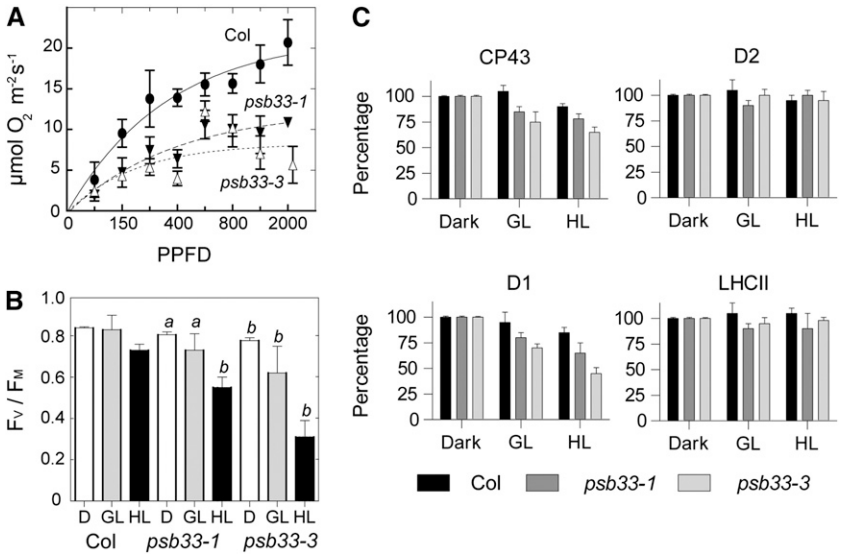

Figure 4. A, PSII activity in *psb33* mutants. Oxygen-evolving activity as a function of light intensity (PPFD) is shown. Oxygen release was measured in vivo at varied light from the wild type (Col; black circles), *psb33-1* (black triangles), and *psb33-3* (white triangles). Sample size was $n = 4$, and the SD is indicated by error bars. B, Chl fluorescence analysis of wild-type (Col) and *psb33* leaves. The efficiency of PSII photochemistry is displayed as the F_v/F_m value on the *y* axis. Sample size was $n = 10$, and the SD is indicated by error bars; *a* and *b* denote significant differences at $P < 0.05$ and $P < 0.01$, respectively. C, Protein levels of LHCII, D1, D2, and CP43 ($n = 3$) plotted as columns with their SD shown as error bars, where the protein levels from dark-incubated wild-type or mutant plants are set as 100%. GL, Growth light; HL, high light.

D1 protein accumulation (Supplemental Fig. S5E). To address whether the increased ROS levels contributed to the loss of D1, we investigated whether artificially increasing ascorbate levels caused an improvement in the photosynthetic performance index and the D1 abundance in the *psb33-3* mutant (Tóth et al., 2011). A positive effect on the performance index and D1 abundance was observed under low-light conditions in the presence of ascorbate, consistent with the hypothesis that ROS damage contributes to the mutant photosynthetic phenotype (Supplemental Fig. S5, E and F). To ask whether reduced D1 abundance in the *psb33-3* mutant results from altered D1 degradation or synthesis, we tested the effect of the chloroplast protein synthesis inhibitor lincomycin on the photosynthetic activity. At low light, both in the presence or absence of lincomycin, the *psb33-3* mutant showed decreases in D1 levels and photosynthetic performance index (Supplemental Fig. S5, E and F) as compared with the wild type. As expected (Ellis and Hartley, 1971), these effects suggest not only that PSII damage is elevated but also that PSII repair is impaired. Taken together with the observation that *psb33-3* plants have greater D1 degradation and lower photosynthetic activity in low light in the absence of lincomycin, these results suggest that the main effect is on the efficiency of the repair cycle. Further evidence that the repair cycle is affected is shown by a positive effect on *psb33-3* when incubated with the reactive oxygen scavenger ascorbic acid (Nishiyama and Murata, 2014). The growth phenotype of *psb33* mutant plants at low and high light correlates well with the results above (Supplemental Fig. S5G).

PSB33 Influences NPQ

The observations that *psb33* mutant plants retain a reduced amount of PSII-LHCII supercomplexes, have altered electron transfer within PSII, and are sensitive to photoinhibition suggest a role for PSB33 in preventing PSII damage and/or enhancing the stability of this complex. This led us to hypothesize that NPQ, as a key regulatory component, could be affected in the *psb33* mutants.

NPQ kinetics were measured at three different light intensities (300, 700, and 1,300 PPFD), and the plants carrying severe *psb33* alleles displayed an initial increase (60–180 s) and a subsequent decrease (180–600 s) in NPQ compared with the wild type at 300 and 700 PPFD. To our great surprise, NPQ of *psb33* mutant plants resembled that of wild-type plants at 1,300 PPFD (Fig. 5A). The effect on NPQ observed with the mutant could be related to the observed loss of the PSII-LHCII supercomplex in the *psb33* mutants, but we were interested to determine whether the PSB33 mutant also displayed other phenotypes indicative of impaired NPQ, such as an altered luminal pH, increased activity of the violaxanthin cycle, and state transitions (Niyogi et al., 1998; Kanazawa and Kramer, 2002; Pesaresi et al., 2009).

To investigate these parameters, we first analyzed the proton gradient (ΔpH) and transmembrane potential (ΔΨ) in the lumen by measuring the electrochromic band shift at 515 nm. No significant difference in proton-motive force, ΔpH, or ΔΨ was observed between the *psb33-3* mutant and the wild type (Table I). To further test whether the violaxanthin cycle was altered, we measured the deepoxidation state of violaxanthin by extracting pigments from leaves exposed to 120, 300, and 1,300 PPFD. In fact, the deepoxidation state was 10 times lower in the *psb33-3* mutant than in the wild type when exposed to 700 PPFD (Fig. 5B). That *psb33* mutants show a relatively moderate change in NPQ activity can be put in comparison with *npq1*, an Arabidopsis zeaxanthin null mutant, that still retains 25% of the NPQ relative to the wild type (Niyogi et al., 1998). Furthermore, reflecting the almost normal NPQ at 1,300 PPFD, the deepoxidation state of the *psb33-3* mutant at this light intensity was similar to that of wild-type plants (Fig. 5B).

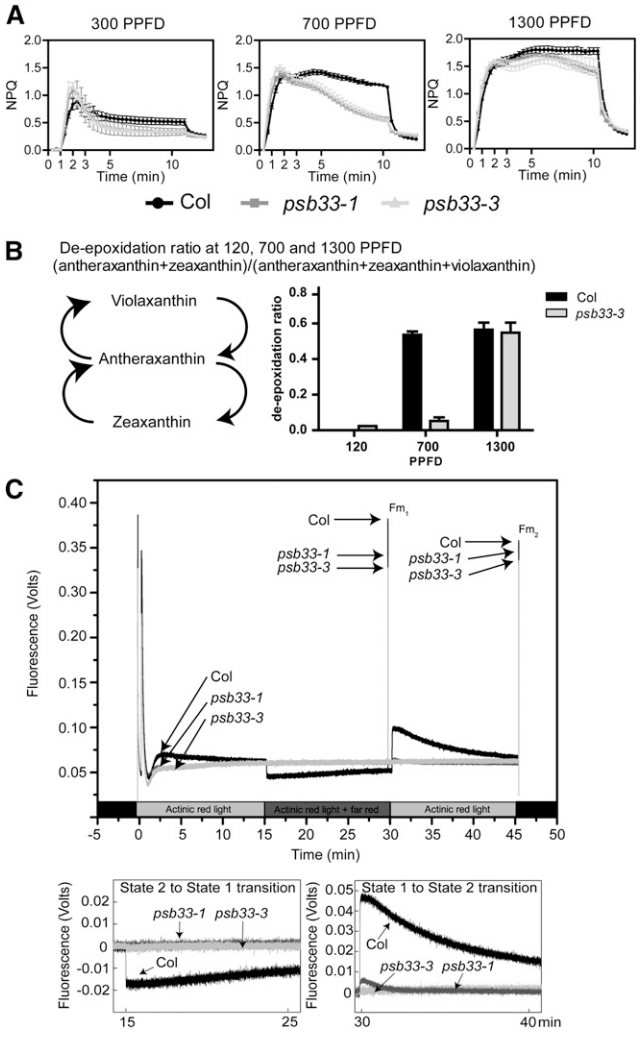

Figure 5. Efficiency of light energy that is absorbed and distributed between PSII and quenching. A, Chl fluorescence analysis of wild-type (Col) and *psb33* leaves. Plants were grown under 120 PPFD and were dark acclimated for a minimum of 12 h before measurements in 300, 700, or 1,300 PPFD. The NPQ is displayed on the *y* axis. Sample size was $n = 5$ to 10, and the SD is indicated by error bars. B, Pigment analysis of wild-type (Col) and *psb33-3* leaves. The deepoxidation rate was calculated from the amount of violaxanthin, antheraxanthin, and zeaxanthin pigments ($\mu g\ m^{-2}$) extracted from leaves that were dark acclimated for a minimum of 12 h and subsequently exposed to 0, 120, 700, or 1,300 PPFD. C, LHCII state transition. Top, Fluorescence response curve displaying state transition, as measured in dark-adapted leaves exposed to 100 PPFD favoring either PSII (red) or PSI (far red). Bottom, Fuorescence response curves when illumination of light is changed to favor PSI (state 2-to-state 1 transition; left) and when illumination of light is changed back to favor PSII (state 1-to-state 2 transition; right).

Yet another component of NPQ is how plants regulate photosynthesis by state transition (i.e. redistribution of LHCII between the two photosystems; Lunde et al., 2000; Depège et al., 2003; Shapiguzov et al., 2010; Tikkanen et al., 2011). The state transition processes are influenced by the phosphorylation and dephosphorylation of various PSII proteins and the trimeric LHC (Fristedt and Vener, 2011; Samol et al., 2012). The thylakoid Ser/Thr-protein kinases STN7 and STN8, which phosphorylate LHCII and PSII, respectively, were shown previously to be activated by a reduced plastoquinone pool (Samol et al., 2012). We measured the phosphorylation status of the thylakoid membrane proteins LHCII, D1, D2, and CP43 in plants acclimated to dark, 120 PPFD, and 800 PPFD (Supplemental Fig. S6). Phosphorylation of LHCII was only slightly altered in *psb33* mutants. This indicates that reduction of the plastoquinone pool is not limited by a loss of PSB33 and suggests that the LHC state transition is functional in *psb33-3*. On the other hand, the phosphorylation level of PSII was reduced in *psb33-1* and *psb33-3* mutants relative to the wild type, and we propose that the lack of the PSII-LHCII supercomplex is the limiting factor for PSII phosphorylation in the mutant. In contrast to these findings, the measured state transition was greatly altered in the mutants. The state transition from state 1 to state 2 and from state 2 to state 1 was very low in the leaky *psb33-1* mutant (with 15% residual PSB33; Fig. 1C) and completely absent in the null *psb33-3* mutant (Fig. 5C).

DISCUSSION

ROS production is a natural result of oxygenic photosynthesis. The PSII protein complex is especially susceptible to damage by ROS, and photosynthetic organisms have evolved a variety of mechanisms to optimize photosynthesis by regulating the absorption or distribution of light energy from the LHC. There are two well-documented mechanisms: (1) NPQ can quench the light energy harvested by the light-harvesting antenna (Ruban and Murchie, 2012; Niyogi and Truong, 2013); and (2) state transition, where LHCII is either associated with PSII or PSI to balance the electron transfer rate to and from each complex (Depège et al., 2003).

We provide evidence that a previously uncharacteized protein, which we named PSB33, has a role in the structural organization of PSII and mediates the LHCII association with this complex. The influence of PSB33 on PSII maintenance is indicated by the observation that *psb33* mutant plants have a lower amount of the PSII-LHCII complex under growth-light (130 PPFD) conditions (Fig. 3). Furthermore, the wild-type PSB33 is associated with the D1-containing complexes: the PSII-LHCII supercomplex, PSII dimers, PSII monomers, and CP43-less PSII monomers (Fig. 3). Based on the reduction in LHCII-containing PSII-LHCII in the mutant and the localization of PSB33 in PSII core protein-containing complexes, we hypothesize that PSB33 is situated close to PSII and is located between LHCII, CP43, and the other PSII core proteins and could mediate the interaction between LHCII and PSII core complexes. This is supported by coimmunoprecipitation and cross-linker experiments (Supplemental Fig. S4).

In addition to its role in PSII-LHCII supercomplex maintenance, several lines of evidence suggest a role for PSB33 in optimizing photosynthesis by influencing

electron transfer at PSII, the processes of NPQ, and state transitions. This is indicated by an altered PSII electron transfer and fast reduction of NPQ in mutant plants exposed to 300 and 700 PPFD (Fig. 5A). In addition, the *psb33* mutants lacked state transitions while retaining a functional LHCII phosphorylation apparatus, albeit with impaired PSII phosphorylation. The finding that *psb33* mutants show effects in all three major pathways that plants use to avoid light stress is very striking. For example, the state transition mutant *stn7* shows only a slight change of NPQ and electron transfer and no growth phenotype under constant light (Bellafiore et al., 2005; Lambrev et al., 2010). A *psbw* mutant reveals low levels of PSII supercomplexes, an abnormal PSII electron transfer, and a slow-growth phenotype but no changes in state transition or NPQ (García-Cerdán et al., 2011). Mutants affected in NPQ, such as the zeaxanthin-deficient mutant *npq1*, show a strongly inhibited NPQ but no changes in electron transfer of PSII in either low or high light and no growth phenotype (Havaux et al., 2000). These findings suggest that PSB33 could have a role in regulating and optimizing photosynthesis in all three major pathways to avoid photoinhibition, depending on light fluence.

That PSB33 is notated to be phosphorylated in PhosPhAt 4.0 and in the Arabidopsis PSB33 ortholog in *Chlamydomonas reinhardtii* (Durek et al., 2010; Wang et al., 2014) suggests the hypothesis that the phosphorylation and dephosphorylation of PSB33 is a trigger for LHCII deassociation and association to PSII. A role for PSB33 in the avoidance of light stress is further indicated by the slower PSII electron transfer and reduced growth rate under high-light conditions (Supplemental Fig. S5G).

Our topology experiments suggest that the N-terminal soluble domain of PSB33 faces the stroma, where it may interact with one or more partners. PSB33 and orthologs lack the residues required to bind the iron-sulfur cluster characteristic of related Rieske proteins. This observation, combined with the presence of a transmembrane region with similarity to the LHC superfamily, which could promote interaction with the LHC, supports a structural or regulatory role rather than a catalytic role. The diverse mutant phenotypes associated with the loss of PSB33 and the absence of an orthologous protein in cyanobacteria are consistent with the hypothesis that PSB33 contributes to a plant lineage-specific environmental adaptation that facilitates the association of LHCII with PSII and influences both NPQ and state transitions.

MATERIALS AND METHODS

Plant Material

Arabidopsis (*Arabidopsis thaliana*) Col and Landsberg *erecta* wild-type and mutant plants were obtained from the Arabidopsis Biological Resource Center (www.Arabidopsis.org). Plants were grown in an 8-h-light (150 PPFD)/16-h-dark cycle in either a Conviron or Percival (controlled environments limited) growth chamber (model MTR26 or E30BHOC8). The plants were screened by PCR for homozygosity of the T-DNA insertion using primers 097813_F and 097813_R for SALK_097813, GT25677_F and GT25677_R for GT25677, 574D02_F and 574D02_R for 574D02, and T-DNA left border primers LBb1, Ds3-4, and o8409 for SALK, CSHL, and GABI-Kölner Arabidopsis T-DNA lines, respectively. DNA fragments were amplified by 30 cycles of denaturation at 94°C for 30 s, annealing at 63°C for 45 s, and extension at 72°C for 3 min.

Structural Analyses and Homology Searches

Plant homologs of PSB33 were identified by a BLAST search at the National Center for Biotechnology Information (http://www.ncbi.nlm.nih.gov). Intracellular location and membrane topology were predicted via a suite of prediction programs (ARAMEMNON; Schwacke et al., 2003). Amino acid sequences were aligned in Jalview using ClustalW and Gblock sorting before constructing a phylogenetic tree (iTOL). A structural homology model of Arabidopsis PSB33 was built from its amino acid sequence using I-TASSER (Roy et al., 2010) with Protein Data Bank code h319. Protein sequence alignments between PSB33 (At1g71500) and closely related homologs from land plants, green algae, and cyanobacteria were created with MUSCLE (Edgar, 2004) and visualized with ESPript (Gouet et al., 1999). Transmembrane regions were predicted with a strict cutoff in DAS (Cserzö et al., 1997). The neighbor-joining tree of PSB33 orthologs encoded in the genomes of land plants and green algae was constructed with MEGA.

Construction of *PSB33-phoA-lacZα* Sandwich Fusions

Translational fusions between *PSB33* and the dual PhoA-LacZα reporter (Alexeyev and Winkler, 1999) were engineered at the 5′ and 3′ sides of the putative transmembrane region. The gene encoding the PhoA-LacZα reporter was amplified from pMA650 (Alexeyev and Winkler, 1999) using PhoA_*Bam*HI_F and LacZ_*Age*I_R. The 5′ region of *PSB33* was amplified using Psb33_*Nco*I and either Psb33_*Bam*HI_1 for construct 1, Psb33_*Bam*HI_2 for construct 2, or Psb33_*Bam*HI_3 for construct 3. The 3′ region of *PSB33* was amplified using Psb33_*Xba*I and either Psb33_*Age*I_1 for construct 1, Psb33_*Age*I_2 for construct 2, or Psb33_*Age*I_3 for construct 3. For constructs 1 to 3, a four-way ligation was performed between pBAD22 (digested *Nco*I/*Xba*I), the 5′ fragment of *PSB33* (digested *Nco*I/*Bam*HI), the PhoA-LacZα reporter (digested *Bam*HI/*Age*I), and the 3′ fragment of *PSB33* (digested *Age*I/*Xba*I). For the C-terminal fusion (construct 4), a three-way ligation was performed between pBAD22 (digested *Nco*I/*Xba*I), *PSB33* amplified with primers PSB33_*Nco*I and PSB33_*Bam*HI_4 (digested *Nco*I/*Bam*HI), and the PhoA-LacZα reporter amplified with primers PhoA_*Bam*HI_F and LacZ_*Xba*I_stop_R (digested *Bam*HI/*Xba*I). The sequence-verified constructs were transformed into *Escherichia coli* NEB alpha cells (New England Biolabs) and plated on dual indicator plates as described (Alexeyev and Winkler, 1999) except that 0.2% (w/v) Ara was used for induction instead of isopropylthio-β-galactoside.

Complementation of *psb33-1* with the At1g71500 Gene

For transgenic complementation analysis, a 2-kb DNA fragment, including a 0.7-kb region upstream of the ATG site, the full genomic *PSB33* sequence, and a 0.2-kb 3′ UTR, was amplified by using primers PSB33_F and PSB33_R and cloned into the vector pEGAD (The Arabidopsis Information Resource). The resulting pEGAD-*PSB33* clone was introduced by electroporation into *Agrobacterium tumefaciens* strain AGL0. Transformation of the homozygous *psb33-1* mutant was carried out using the floral dip method (Clough and Bent, 1998). Transformants were selected on soil with the herbicide BASTA (120 mg L^{-1}; Bayer Scientific; Chemical Abstracts Service no. 77182-82-2). The T1 and T2 generations of transformants were assayed by phenotypic analysis, blue native gel electrophoresis, and immunodetection.

Fluorescence Microscopy

A complementary DNA clone (U17348) for At1g71500 was obtained from the Arabidopsis Biological Resource Center, and the open reading frame minus its stop codon was amplified using primers U17348_F and U17348_R. The obtained product was reamplified using primers U17348_RE_F and U17348_RE_R, cloned in the Gateway entry vector PDONR221, and fused in frame to the 5′ end of a GFP in the PMDC83 destination vector (Curtis and Grossniklaus, 2003; Life Technologies). The destination vector was transformed into *A. tumefaciens* strain LBA4404 and infected into tobacco (*Nicotiana tabacum*). PSB33-GFP expression in infected tobacco leaves was imaged after 48 h using a confocal laser scanning microscope (Olympus Fluoview FV1000). Fluorescence from GFP was detected by excitation at 488 nm and a 510-nm emission filter. Chl autofluorescence was detected using an excitation wavelength of 543 nm and a 633-nm long-pass emission filter.

Arabidopsis Plant Tissue Preparations, Electrophoresis, and Immunodetection

Plant tissue, chloroplasts, stroma, thylakoid membranes, PSII-enriched membranes, PSII-LHCII, PSII cores, and lumen were isolated from Arabidopsis or spinach (*Spinacia oleracea*) as described (Spetea et al., 2004). Intact chloroplasts were isolated by Percoll gradient centrifugation, and thylakoid membranes were isolated and fractionated by Suc gradient centrifugation. Proteins were separated according to Lu et al. (2011a).

Antibody Production

Denaturing PAGE and immunodetection were performed as described (Aro et al., 2005; Fristedt et al., 2009). An antibody specific for PSB33 (α_1-PSB33) was produced by immunization of rabbits with a peptide (corresponding to amino acids 274–287 of PSB33) and purified by affinity chromatography (Innovagen). A second antibody (α_2-PSB33) specific for PSB33 was produced by immunization of rabbits with a recombinant protein corresponding to amino acids 61 to 242 of PSB33 (Agrisera TEF5 AS121852). Antibodies for subunit IV of the cytochrome b_6f complex were raised against its C-terminal region, and those for the Rieske subunit cytochrome b_6f complex iron-sulfur subunit (PetC) were raised against the entire mature protein of *Chlamydomonas reinhardtii*. Antibodies against CP43 (AS06 110), α1-D1 (AS10704), α2-D1 (AS11 1786), Lhca1 (AS01 005), Lhca2 (AS01 006), Lhcb1 (AS01 004), Lhcb2 (AS01 003), Lhcb4 (AS04 045), the large subunit of Rubisco (AS03 037-10), PsaA (AS06 172), cytochrome *f* (AS06 119), PetC (AS08 330), actin (ABIN619544), and PsaN (AS06 109) were obtained from Agrisera. Immunoreactive proteins were visualized using the SuperSignal WestPico Horseradish Peroxidase detection kit (Thermo Scientific) as directed by the manufacturer. For immunoprecipitation, chloroplasts from 3-week-old wild-type Col and *psb33-1* mutant plants were isolated and gradient purified as described. The chloroplasts were resuspended in solubilization buffer (20 mM Tricine-NaOH, pH 7.8, 5 mM $MgCl_2$, and 100 mM Suc) containing 10 mM *n*-dodecyl β-D-maltoside and incubated at room temperature for 15 min. The insoluble membrane particles were removed by centrifugation at 4°C at 14,000*g* for 30 min, and the protein concentration was measured on the resulting supernatant by using the Lowry protein assay as described (Lowry et al., 1951). Pierce cross-link magnetic beads were coupled to α_1-PSB33 according to the manufacturer's instructions (Pierce Crosslink Magnetic IP/Co-IP Kit 88805). The beads were incubated with 50 μL of solubilized chloroplasts at a protein concentration of 2 μg μL^{-1} for 30 min with slow rotation at room temperature. Washing and elution of proteins coimmunoprecipitated with PSB33 were performed according to the manufacturer's instructions (Pierce Crosslink Magnetic Co-IP Kit 88805). The eluted proteins were separated on a 15% (v/v) polyacrylamide gel and stained with silver as described (Goulas et al., 2006). In-gel digestion of selected protein bands was performed as described (Fristedt and Vener, 2011).

Heme-Specific Staining

TMBZ staining was done on 12% (w/v) SDS gels (run as described above). The samples were solubilized for 30 min on ice with 50 mM dithiothreitol in sample buffer (note, not 2-mercaptoethanol). TMBZ was dissolved in methanol in the dark at room temperature, and after dissolving, NaOAc (CH_3COONa; 1 M, pH 5) was added to the TMBZ solution at final concentrations of 0.25 M and 6.3 mM TMBZ. The gels were incubated for 45 min in the dark at 4°C. To reveal the heme bands, H_2O_2 was added at a final concentration of 30 mM. After approximately 10 min to stop the development, the H_2O_2 solution was exchanged to water.

Blue Native Gel and 2D Electrophoresis

Thylakoid membranes were resuspended in 20% (w/v) glycerol and 25 mM BisTris-HCl, pH 7, to a Chl concentration of 2 mg mL^{-1}. An equal volume of 1.5% (w/v) *n*-dodecyl β-D-maltoside in resuspension buffer was added, and the mixture was incubated on ice for 10 min. After centrifugation at 14,000*g* for 30 min, the supernatant was supplemented with 0.1 volume of sample buffer (100 mM BisTris-HCl, pH 7, 0.5 M ε-amino-*n*-caproic acid, 30% [w/v] Suc, and 50 mg mL^{-1} Serva Blue G) and subjected to blue native gel electrophoresis with a gradient of 5% to 13.5% (v/v) polyacrylamide gel on the separation gel (Fristedt and Vener, 2011). For separation of proteins in the second dimension, individual lanes were excised from the first-dimension gel and incubated with 5% (v/v) β-mercaptoethanol in SDS sample buffer for 30 min at room temperature prior to SDS-PAGE on 15% (v/v) polycrylamide gels. For immunodetection, the native gels were incubated in blotting buffer (25 mM Tris, 192 mM Gly, and 10% [v/v] methanol) for 30 min before the transfer of proteins to a polyvinylidene difluoride membrane for 120 min at 30 mA gel^{-1} (Immobilon; Millipore).

After transfer, the membranes were blocked with 10% (w/v) skim milk. An incubation with the first antibody was done overnight at 4°C. The membranes were washed six times using Tween Tris-buffered saline and then incubated at room temperature with horseradish peroxidase-conjugated secondary antibody for 1 h. The membranes were washed six times with Tween Tris-buffered saline and the immunoreactive proteins were visualized following a 10-min incubation with detecting reagents from the SuperSignal WestPico Horseradish Peroxidase detection kit (Thermo Scientific).

Liquid Chromatography and Mass Spectrometry

The bands indicated by arrows in Supplemental Figure S4A were excised from the gel and treated with trypsin (sequencing-grade modified trypsin; Promega) according to Shevchenko et al. (2002). Peptides were analyzed as described previously (Hsieh et al., 2013) using a nanoAcquity UltraPerformance HPLC system (Waters) coupled to a Waters Xevo quadrupole time-of-flight mass spectrometer. Ultra-performance liquid chromatography was performed using a 5-μm Symmetry C18, 180-μm × 20-mm reverse-phase trap column in line with a 1.7-μm BEH130, 75-μm × 100-mm reverse-phase C18 analytical column. Protein Lynx Global Server (version 2.4; Waters) was used to process the liquid chromatography-mass spectrometry raw data and to determine protein identifications (Supplemental Fig. S4).

Oxygen-Evolving Activity

In vivo steady-state and single-burst oxygen-evolving activity was measured using a gas-phase oxygen electrode system (LD1/2 Electrode chamber; Hansatech) in 11.3-mm^2 leaf discs using a Clark-type electrode (S1 Oxygen electrode disc; Hansatech) and a red light-emitting diode light system (LH36/2R; Hansatech) at various light conditions.

Pigment Analysis

The Chl content and pigments of whole leaves were either determined by extraction in 80% (v/v) acetone and measured in a spectrophotometer at wavelengths of 646.6 and 663.6 nm according to Porra (2002) or determined by extraction in methanol and subsequently measured by high performance liquid chromatography.

Chl Fluorescence and Electrochromic Band-Shift Measurements

Chl fluorescence was measured using a pulse-amplitude fluorometer (dual PAM-100; Walz). Its parameters were analyzed according to standard techniques (Yin et al., 2012), and curves were obtained using light intensities of 300, 700, and 1,300 PPFD. For the data presented in Table I, plants were dark adapted for a minimum of 12 h, and measurements were taken every 20 s for the first 3 min and then every 1 min for 22 min until a steady state of photosynthesis was reached at 25 min. Otherwise, plants were dark adapted for a minimum of 12 h, and measurements were taken every 20 s for up to 10 min. For the data presented in Supplemental Figure S5, plants were dark adapted for a minimum of 12 h before being exposed to high light (800 PPFD), and measurements were taken after 15 min of dark adaptation from long-term dark-adapted plants and from plants exposed to either 2 or 4 h of light illumination. The electrochromic band shift was measured using a dual PAM-100 setup with a 515/535 module. Plants were dark adapted for a minimum of 30 min, and leaves were illuminated for 3 min with 166, 660, 1,287, or 1,952 PPFD, after which proton-motive force, ΔpH, and $\Delta\Psi$ values were determined as described (Cruz et al., 2005). State transition was measured using a dual PAM-100 fluorometer according to Lunde et al. (2000). The excitation wavelength of actinic red light had a peak at 628 nm, and that of far-red light had a peak at 716 nm. The light intensity used was 100 PPFD.

Oxidative Stress Measurements

Histochemical staining for H_2O_2 and superoxide was detected by incubation with either 3,3′-diaminobenzidine (Sigma-Aldrich) or nitroblue tetrazolium (Sigma-Aldrich) for 2 h and subsequently exposed to dark or 1 or 3 h of high light (800 PPFD) as described previously (Suorsa et al., 2012). Visualization of singlet

oxygen was obtained by fluorescence microscopy on leaves incubated in 330 nM Singlet Oxygen Sensor Green (Sigma-Aldrich) for 2 h and subsequently exposed to dark or 1 or 3 h of high light (800 PPFD) as described previously (Lu et al., 2011a).

Antioxidant and Lincomycin in Vivo Incubation

Leaves that were dark acclimated for 12 h were then incubated with or without 20 mM ascorbic acid and illuminated first with low light (50 PPFD) for 2 h and then subsequently with high light (800 or 1,000 PPFD) for varying time periods. Photosynthetic parameters were determined from fluorescence data recorded at 0, 2, 3, 4, and 5 h using a PEA fluorometer (Hansatech). D1 levels were measured by immunodetection from total leaf protein extraction. Each time point consists of an extraction from three individual leaves.

Sequence data from this article can be found in the GenBank/EMBL database or the Arabidopsis Genome Initiative database under the following accession numbers: PSB33 (At1g71500, 843491); *psb33-1* (SALK_098173); *psb33-2* (CSHL_GT25677); and *psb33-3* (GABI_574D02).

Supplemental Data

The following supplemental materials are available.

Supplemental Figure S1. Transgenic complementation.

Supplemental Figure S2. Immunodetection of thylakoid membrane proteins.

Supplemental Figure S3. Sequence and topology analysis of PSB33.

Supplemental Figure S4. PSB33 protein interactions using a PSB33-specific antibody.

Supplemental Figure S5. Oxidatively damaged thylakoid membrane proteins and D1 repair process.

Supplemental Figure S6. Thylakoid protein phosphorylation.

Supplemental Table S1. Thylakoid protein transcriptional abundance estimates.

ACKNOWLEDGMENTS

We thank Linda Savage and Joseph A. Loo for technical support; Jean David Rochaix, Cornelia Spetea Wiklund, and Eevi Rintamäki for helpful advice; Patrice Hamel for providing the LTO1-SSS and LTO1-WCSHC constructs; and Herbert Winkler for providing pMA650; the members of University of California, Los Angeles Molecular Instrumentation Center for use of the Orbitrap instrument; and the University of California, Los Angeles-Department of Energy Protein Expression Technology Center for assistance with cloning, expression, and purification of PSB33 recombinant protein.

Received November 7, 2014; accepted December 14, 2014; published December 15, 2014.

LITERATURE CITED

Ajjawi I, Lu Y, Savage LJ, Bell SM, Last RL (2010) Large-scale reverse genetics in Arabidopsis: case studies from the Chloroplast 2010 Project. Plant Physiol **152:** 529–540

Alexeyev MF, Winkler HH (1999) Membrane topology of the *Rickettsia prowazekii* ATP/ADP translocase revealed by novel dual *pho-lac* reporters. J Mol Biol **285:** 1503–1513

Aro EM, Suorsa M, Rokka A, Allahverdiyeva Y, Paakkarinen V, Saleem A, Battchikova N, Rintamäki E (2005) Dynamics of photosystem II: a proteomic approach to thylakoid protein complexes. J Exp Bot **56:** 347–356

Barber J, Ferreira KN, Maghlaoui K, Iwata S (2004) Structural model of the oxygen-evolving centre of photosystem II with mechanistic implications. Phys Chem Chem Phys **6:** 4737–4742

Bellafiore S, Barneche F, Peltier G, Rochaix JD (2005) State transitions and light adaptation require chloroplast thylakoid protein kinase STN7. Nature **433:** 892–895

Bernal M, Casero D, Singh V, Wilson GT, Grande A, Yang H, Dodani SC, Pellegrini M, Huijser P, Connolly EL, et al (2012) Transcriptome sequencing identifies *SPL7*-regulated copper acquisition genes *FRO4*/*FRO5* and the copper dependence of iron homeostasis in *Arabidopsis*. Plant Cell **24:** 738–761

Clough SJ, Bent AF (1998) Floral dip: a simplified method for Agrobacterium-mediated transformation of *Arabidopsis thaliana*. Plant J **16:** 735–743

Cruz JA, Avenson TJ, Kanazawa A, Takizawa K, Edwards GE, Kramer DM (2005) Plasticity in light reactions of photosynthesis for energy production and photoprotection. J Exp Bot **56:** 395–406

Cserzö M, Wallin E, Simon I, von Heijne G, Elofsson A (1997) Prediction of transmembrane alpha-helices in prokaryotic membrane proteins: the dense alignment surface method. Protein Eng **10:** 673–676

Curtis MD, Grossniklaus U (2003) A Gateway cloning vector set for high-throughput functional analysis of genes in planta. Plant Physiol **133:** 462–469

Depège N, Bellafiore S, Rochaix JD (2003) Role of chloroplast protein kinase Stt7 in LHCII phosphorylation and state transition in Chlamydomonas. Science **299:** 1572–1575

Durek P, Schmidt R, Heazlewood JL, Jones A, MacLean D, Nagel A, Kersten B, Schulze WX (2010) PhosPhAt: the *Arabidopsis thaliana* phosphorylation site database. An update. Nucleic Acids Res **38:** D828–D834

Edgar RC (2004) MUSCLE: multiple sequence alignment with high accuracy and high throughput. Nucleic Acids Res **32:** 1792–1797

Ellis RJ, Hartley MR (1971) The sites of synthesis of chloroplast proteins. Biochem J **124:** 11P–12P

Fristedt R, Carlberg I, Zygadlo A, Piippo M, Nurmi M, Aro EM, Scheller HV, Vener AV (2009) Intrinsically unstructured phosphoprotein TSP9 regulates light harvesting in *Arabidopsis thaliana*. Biochemistry **48:** 499–509

Fristedt R, Vener AV (2011) High light induced disassembly of photosystem II supercomplexes in Arabidopsis requires STN7-dependent phosphorylation of CP29. PLoS ONE **6:** e24565

García-Cerdán JG, Kovács L, Tóth T, Kereïche S, Aseeva E, Boekema EJ, Mamedov F, Funk C, Schröder WP (2011) The PsbW protein stabilizes the supramolecular organization of photosystem II in higher plants. Plant J **65:** 368–381

Gouet P, Courcelle E, Stuart DI, Métoz F (1999) ESPript: analysis of multiple sequence alignments in PostScript. Bioinformatics **15:** 305–308

Goulas E, Schubert M, Kieselbach T, Kleczkowski LA, Gardeström P, Schröder W, Hurry V (2006) The chloroplast lumen and stromal proteomes of *Arabidopsis thaliana* show differential sensitivity to short- and long-term exposure to low temperature. Plant J **47:** 720–734

Hamel PP, Dreyfuss BW, Xie Z, Gabilly ST, Merchant S (2003) Essential histidine and tryptophan residues in CcsA, a system II polytopic cytochrome c biogenesis protein. J Biol Chem **278:** 2593–2603

Havaux M, Bonfils JP, Lütz C, Niyogi KK (2000) Photodamage of the photosynthetic apparatus and its dependence on the leaf developmental stage in the *npq1* Arabidopsis mutant deficient in the xanthophyll cycle enzyme violaxanthin de-epoxidase. Plant Physiol **124:** 273–284

Hsieh SI, Castruita M, Malasarn D, Urzica E, Erde J, Page MD, Yamasaki H, Casero D, Pellegrini M, Merchant SS, et al (2013) The proteome of copper, iron, zinc, and manganese micronutrient deficiency in *Chlamydomonas reinhardtii*. Mol Cell Proteomics **12:** 65–86

Kanazawa A, Kramer DM (2002) In vivo modulation of nonphotochemical exciton quenching (NPQ) by regulation of the chloroplast ATP synthase. Proc Natl Acad Sci USA **99:** 12789–12794

Karamoko M, Cline S, Redding K, Ruiz N, Hamel PP (2011) Lumen Thiol Oxidoreductase1, a disulfide bond-forming catalyst, is required for the assembly of photosystem II in *Arabidopsis*. Plant Cell **23:** 4462–4475

Karpowicz SJ, Prochnik SE, Grossman AR, Merchant SS (2011) The GreenCut2 resource, a phylogenomically derived inventory of proteins specific to the plant lineage. J Biol Chem **286:** 21427–21439

Lambrev PH, Nilkens M, Miloslavina Y, Jahns P, Holzwarth AR (2010) Kinetic and spectral resolution of multiple nonphotochemical quenching components in Arabidopsis leaves. Plant Physiol **152:** 1611–1624

Lowry OH, Rosebrough NJ, Farr AL, Randall RJ (1951) Protein measurement with the Folin phenol reagent. J Biol Chem **193:** 265–275

Lu Y, Hall DA, Last RL (2011a) A small zinc finger thylakoid protein plays a role in maintenance of photosystem II in *Arabidopsis thaliana*. Plant Cell **23:** 1861–1875

Lu Y, Savage LJ, Ajjawi I, Imre KM, Yoder DW, Benning C, Dellapenna D, Ohlrogge JB, Osteryoung KW, Weber AP, et al (2008) New connections across pathways and cellular processes: industrialized mutant screening reveals novel associations between diverse phenotypes in Arabidopsis. Plant Physiol **146:** 1482–1500

Lu Y, Savage LJ, Larson MD, Wilkerson CG, Last RL (2011b) Chloroplast 2010: a database for large-scale phenotypic screening of Arabidopsis mutants. Plant Physiol **155:** 1589–1600

Lunde C, Jensen PE, Haldrup A, Knoetzel J, Scheller HV (2000) The PSI-H subunit of photosystem I is essential for state transitions in plant photosynthesis. Nature **408:** 613–615

Martins BM, Svetlitchnaia T, Dobbek H (2005) 2-Oxoquinoline 8-monooxygenase oxygenase component: active site modulation by Rieske-[2Fe-2S] center oxidation/reduction. Structure **13:** 817–824

Merchant SS, Prochnik SE, Vallon O, Harris EH, Karpowicz SJ, Witman GB, Terry A, Salamov A, Fritz-Laylin LK, Maréchal-Drouard L, et al (2007) The Chlamydomonas genome reveals the evolution of key animal and plant functions. Science **318:** 245–250

Munné-Bosch S, Queval G, Foyer CH (2013) The impact of global change factors on redox signaling underpinning stress tolerance. Plant Physiol **161:** 5–19

Nishiyama Y, Murata N (2014) Revised scheme for the mechanism of photoinhibition and its application to enhance the abiotic stress tolerance of the photosynthetic machinery. Appl Microbiol Biotechnol **98:** 8777–8796

Niyogi KK, Grossman AR, Björkman O (1998) *Arabidopsis* mutants define a central role for the xanthophyll cycle in the regulation of photosynthetic energy conversion. Plant Cell **10:** 1121–1134

Niyogi KK, Truong TB (2013) Evolution of flexible non-photochemical quenching mechanisms that regulate light harvesting in oxygenic photosynthesis. Curr Opin Plant Biol **16:** 307–314

Pagliano C, Saracco G, Barber J (2013) Structural, functional and auxiliary proteins of photosystem II. Photosynth Res **116:** 167–188

Pesaresi P, Hertle A, Pribil M, Kleine T, Wagner R, Strissel H, Ihnatowicz A, Bonardi V, Scharfenberg M, Schneider A, et al (2009) *Arabidopsis* STN7 kinase provides a link between short- and long-term photosynthetic acclimation. Plant Cell **21:** 2402–2423

Porra RJ (2002) The chequered history of the development and use of simultaneous equations for the accurate determination of chlorophylls *a* and *b*. Photosynth Res **73:** 149–156

Punta M, Coggill PC, Eberhardt RY, Mistry J, Tate J, Boursnell C, Pang N, Forslund K, Ceric G, Clements J, et al (2012) The Pfam protein families database. Nucleic Acids Res **40:** D290–D301

Roy A, Kucukural A, Zhang Y (2010) I-TASSER: a unified platform for automated protein structure and function prediction. Nat Protoc **5:** 725–738

Ruban AV, Murchie EH (2012) Assessing the photoprotective effectiveness of non-photochemical chlorophyll fluorescence quenching: a new approach. Biochim Biophys Acta **1817:** 977–982

Samol I, Shapiguzov A, Ingelsson B, Fucile G, Crèvecoeur M, Vener AV, Rochaix JD, Goldschmidt-Clermont M (2012) Identification of a photosystem II phosphatase involved in light acclimation in *Arabidopsis*. Plant Cell **24:** 2596–2609

Schwacke R, Schneider A, van der Graaff E, Fischer K, Catoni E, Desimone M, Frommer WB, Flügge UI, Kunze R (2003) ARAMEMNON, a novel database for Arabidopsis integral membrane proteins. Plant Physiol **131:** 16–26

Shapiguzov A, Ingelsson B, Samol I, Andres C, Kessler F, Rochaix JD, Vener AV, Goldschmidt-Clermont M (2010) The PPH1 phosphatase is specifically involved in LHCII dephosphorylation and state transitions in Arabidopsis. Proc Natl Acad Sci USA **107:** 4782–4787

Shevchenko A, Chernushevic I, Shevchenko A, Wilm M, Mann M (2002) "De novo" sequencing of peptides recovered from in-gel digested proteins by nanoelectrospray tandem mass spectrometry. Mol Biotechnol **20:** 107–118

Spetea C, Hundal T, Lundin B, Heddad M, Adamska I, Andersson B (2004) Multiple evidence for nucleotide metabolism in the chloroplast thylakoid lumen. Proc Natl Acad Sci USA **101:** 1409–1414

Suorsa M, Järvi S, Grieco M, Nurmi M, Pietrzykowska M, Rantala M, Kangasjärvi S, Paakkarinen V, Tikkanen M, Jansson S, et al (2012) PROTON GRADIENT REGULATION5 is essential for proper acclimation of *Arabidopsis* photosystem I to naturally and artificially fluctuating light conditions. Plant Cell **24:** 2934–2948

Tikkanen M, Grieco M, Aro EM (2011) Novel insights into plant light-harvesting complex II phosphorylation and 'state transitions.' Trends Plant Sci **16:** 126–131

Tóth SZ, Nagy V, Puthur JT, Kovács L, Garab G (2011) The physiological role of ascorbate as photosystem II electron donor: protection against photoinactivation in heat-stressed leaves. Plant Physiol **156:** 382–392

Wang H, Gau B, Slade WO, Juergens M, Li P, Hicks LM (2014) The global phosphoproteome of *Chlamydomonas reinhardtii* reveals complex organellar phosphorylation in the flagella and thylakoid membrane. Mol Cell Proteomics **13:** 2337–2353

Wegener KM, Bennewitz S, Oelmüller R, Pakrasi HB (2011) The Psb32 protein aids in repairing photodamaged photosystem II in the cyanobacterium *Synechocystis* 6803. Mol Plant **4:** 1052–1061

Yin L, Fristedt R, Herdean A, Solymosi K, Bertrand M, Andersson MX, Mamedov F, Vener AV, Schoefs B, Spetea C (2012) Photosystem II function and dynamics in three widely used *Arabidopsis thaliana* accessions. PLoS ONE **7:** e46206